NASA/TM—1999-209650

IEPC 99–149

Titanium Optics for Ion Thrusters

George C. Soulas
Dynacs Engineering Company, Inc., Brook Park, Ohio

Thomas W. Haag, Michael J. Patterson, and Vincent K. Rawlin
Glenn Research Center, Cleveland, Ohio

December 1999

The NASA STI Program Office . . . in Profile

Since its founding, NASA has been dedicated to the advancement of aeronautics and space science. The NASA Scientific and Technical Information (STI) Program Office plays a key part in helping NASA maintain this important role.

The NASA STI Program Office is operated by Langley Research Center, the Lead Center for NASA's scientific and technical information. The NASA STI Program Office provides access to the NASA STI Database, the largest collection of aeronautical and space science STI in the world. The Program Office is also NASA's institutional mechanism for disseminating the results of its research and development activities. These results are published by NASA in the NASA STI Report Series, which includes the following report types:

- TECHNICAL PUBLICATION. Reports of completed research or a major significant phase of research that present the results of NASA programs and include extensive data or theoretical analysis. Includes compilations of significant scientific and technical data and information deemed to be of continuing reference value. NASA's counterpart of peer-reviewed formal professional papers but has less stringent limitations on manuscript length and extent of graphic presentations.

- TECHNICAL MEMORANDUM. Scientific and technical findings that are preliminary or of specialized interest, e.g., quick release reports, working papers, and bibliographies that contain minimal annotation. Does not contain extensive analysis.

- CONTRACTOR REPORT. Scientific and technical findings by NASA-sponsored contractors and grantees.

- CONFERENCE PUBLICATION. Collected papers from scientific and technical conferences, symposia, seminars, or other meetings sponsored or cosponsored by NASA.

- SPECIAL PUBLICATION. Scientific, technical, or historical information from NASA programs, projects, and missions, often concerned with subjects having substantial public interest.

- TECHNICAL TRANSLATION. English-language translations of foreign scientific and technical material pertinent to NASA's mission.

Specialized services that complement the STI Program Office's diverse offerings include creating custom thesauri, building customized data bases, organizing and publishing research results . . . even providing videos.

For more information about the NASA STI Program Office, see the following:

- Access the NASA STI Program Home Page at *http://www.sti.nasa.gov*

- E-mail your question via the Internet to help@sti.nasa.gov

- Fax your question to the NASA Access Help Desk at (301) 621-0134

- Telephone the NASA Access Help Desk at (301) 621-0390

- Write to:
  NASA Access Help Desk
  NASA Center for AeroSpace Information
  7121 Standard Drive
  Hanover, MD 21076

NASA/TM—1999-209650 IEPC 99–149

Titanium Optics for Ion Thrusters

George C. Soulas
Dynacs Engineering Company, Inc., Brook Park, Ohio

Thomas W. Haag, Michael J. Patterson, and Vincent K. Rawlin
Glenn Research Center, Cleveland, Ohio

Prepared for the
26th International Electric Propulsion Conference
sponsored by the American Institute of Aeronautics and Astronauitcs
Kitakyushu, Japan, October 17–21, 1999

National Aeronautics and
Space Administration

Glenn Research Center

December 1999

This report contains preliminary findings, subject to revision as analysis proceeds.

Available from

NASA Center for Aerospace Information
7121 Standard Drive
Hanover, MD 21076
Price Code: A03

National Technical Information Service
5285 Port Royal Road
Springfield, VA 22100
Price Code: A03

TITANIUM OPTICS FOR ION THRUSTERS

George C. Soulas
Dynacs Engineering Co., Inc.
2001 Aerospace Parkway
Brook Park, Ohio 44142

Thomas W. Haag, Michael J. Patterson, and Vincent K. Rawlin
National Aeronautics and Space Administration
Glenn Research Center
21000 Brookpark Road
Cleveland, Ohio 44135

Abstract

Ion thruster total impulse capability is limited, in part, by accelerator grid sputter erosion. A development effort was initiated to identify a material with a lower accelerator grid volumetric sputter erosion rate than molybdenum, but that could utilize the present NSTAR thruster grid design and fabrication techniques to keep development costs low, and perform as well as molybdenum optics. After comparing the sputter erosion rates of several atomic materials to that of molybdenum at accelerator voltages, titanium was found to offer a 45% reduction in volumetric erosion rates. To ensure that screen grid sputter erosion rates are not higher at discharge chamber potentials, titanium and molybdenum sputter erosion rates were measured at these potentials. Preliminary results showed only a slightly higher volumetric erosion rate for titanium, so that screen grid erosion is insignificant. A number of material, thermal, and mechanical properties were also examined to identify any fabrication, launch environment, and thruster operation issues. Several titanium grid sets were successfully fabricated. A titanium grid set was mounted onto an NSTAR 30 cm engineering model ion thruster and tested to determine optics performance. The titanium optics operated successfully over the entire NSTAR power range of 0.5 to 2.3 kW. Differences in impingement-limited perveances and electron backstreaming limits were found to be due to a larger cold gap for the titanium optics. Discharge losses for titanium grids were lower than those for molybdenum, likely due to a slightly larger titanium screen grid open area fraction. Radial distributions of beam current density with titanium optics were very similar to those with molybdenum optics at all power levels. Temporal electron backstreaming limit measurements showed that titanium optics achieved thermal equilibrium faster than molybdenum optics.

Introduction

The recent success of the NSTAR (i.e. NASA Solar Electric Propulsion Technology Applications Readiness Program) 30 cm ion thruster system on the Deep Space 1 mission has demonstrated the viability of ion propulsion for deep space missions.[1,2] This success has also made ion propulsion a potential candidate for other deep space missions, such as the Comet Nucleus Sample Return, Mercury Orbiter, Neptune Orbiter, Titan Explorer, Europa Lander, and others. However, many of these missions require increasing the thruster's total impulse capability beyond the demonstrated 8200 hours at 2.3 kW.[3] Extending this capability is limited, in part, by charge-exchange sputter erosion of the accelerator grid.[3,4] Although the thruster's total impulse capability is greater than that demonstrated at 2.3 kW for 8200 hours, it is unclear whether the thruster's molybdenum optics can achieve the 50-300% increases in total impulse anticipated for these ambitious missions.[1,3]

Changing the ion optics material to one with a lower volumetric sputter erosion rate is one of several methods that can be used to reduce accelerator grid erosion. To date, there has been considerable effort in developing carbon-carbon optics because of their significantly reduced volumetric sputter erosion rate, and because of other material benefits such as light weight, high strength, and low thermal expansion. Unfortunately, 30 cm carbon-carbon optics have not performed as well as molybdenum optics, have generally been costly, and have required long lead times for fabrication.

A development effort was, therefore, initiated to identify another material with a lower volumetric sputter erosion rate than molybdenum, and to develop these ion optics at a low cost with a performance similar to that of molybdenum. This paper reports on the preliminary results of this development effort,

including the material selection process and initial performance measurements.

Material Selection

To keep development costs low, the candidate material must utilize the NSTAR thruster grid design and fabrication techniques, both of which are briefly described in the first section. The sections thereafter describe the process used to select titanium. Material properties are also examined to determine if titanium could be fabricated, operated, and would survive launch loads.

Optics Design and Fabrication Process

The NSTAR 30 cm ion thruster uses two grids made of perforated, domed molybdenum. The grid dome shape is hydrostatically formed, a process developed by NASA in 1972,[5] and the apertures are photo-chemically etched. The dome shape mitigates material buckling under thermal stresses during thruster operation, and offers mechanical stiffness under vibrational loads during launch. Photo-chemical etching provides a cost-effective method of machining large numbers of apertures to precise tolerances.

Sputter Erosion – Accelerator Grid

The sputter erosion rates of several atomic materials were compared to that of molybdenum to identify materials with low volumetric sputter erosion rates. Alloys were not considered here because their sputter yields are generally unknown. Accelerator grid erosion is primarily from charge-exchange ions at energies approximating accelerator grid voltages. For the NSTAR thruster, these voltages are 150-250 V. Erosion rates due to sputtering from xenon were examined at energies between 100 and 600 eV. To simplify calculations and material comparisons, only sputter yield data for a normal angle of incidence were considered because these data are commonly available. A volumetric sputter erosion rate was calculated for each material, which is determined by the sputter yield divided by the number density of the material:

$$V_{Er} = \frac{Y}{\frac{\varrho}{m}} = \frac{Y \cdot M}{\varrho \cdot N_A} \qquad (1)$$

where V_{Er} is the material volumetric erosion rate per incident ion, Y is the material sputter yield, m is the material atomic mass, ρ is the material density, M is the material atomic mass in amu, and N_A is Avogadro's number.

Because sputter yields tend to vary from investigation to investigation, a material's erosion ratio, which is defined as the volumetric erosion of a material divided by the volumetric erosion of molybdenum:

$$\text{Erosion Ratio} = \frac{V_{Er}}{V_{Er}^{Mo}} \qquad (2)$$

is plotted as a function of xenon energy where the sputter yields of a material and molybdenum were measured within the same investigation. This aided in eliminating some experimental inaccuracies since this ratio requires accurate relative sputter yields and not accurate absolute yields. Sputter yield data were obtained from Rosenberg and Wehner[6] and Blandino et al.[7] Only materials with volumetric erosion rates lower than molybdenum are shown in Fig. 1.

As the figure shows, there are a number of materials with erosion rates lower than molybdenum. Of the metals listed in the figure, zirconium, vanadium, and beryllium were not considered because of their toxicity. Carbon-carbon and niobium were also not considered because they cannot be made with the existing grid fabrication process.

An austenitic stainless steel would have to be used in place of iron because of iron's excessive corrosion at atmospheric conditions and its magnetic properties, which could negatively impact the discharge chamber magnetic circuit. However, an earlier study that utilized stainless steel grids on a 30 cm ion thruster determined that this material buckled under thermally-induced stresses.[8] As a result, stainless steel (or iron) was not considered.

Titanium, however, appeared to be an excellent candidate grid material. It could be made with the existing grid fabrication process and offered a 45% reduction in volumetric erosion rates at accelerator grid potentials.

Sputter Erosion – Screen Grid

If titanium ion optics are to be considered, screen grid sputter erosion rates must not limit thruster total impulse capability. Sputter yield data for titanium and molybdenum by xenon at these low potentials (i.e. ≤ 28 V) are not available for comparison. Although theoretically- and empirically-derived models could be used, these results were not considered in this study since there are no known experimental data to confirm them.

To compare volumetric sputter erosion rates at these low potentials, titanium and molybdenum sputter erosion rates were measured at thruster discharge chamber potentials in a simple xenon discharge. The experimental setup, shown in Fig. 2, included an anode, a hollow cathode surrounded by an enclosure, and a baffle located 1.5 cm downstream of the cathode that acted as the sputtering target. The baffle was a 3.4 cm diameter disk made of either titanium or molybdenum. Discharge and keeper currents were set to 13.0 A and 2.5 A, respectively. The entire discharge was operated in a cryogenically-pumped facility that had a base

pressure of 4.5×10^{-5} Pa (3.4×10^{-7} Torr) and an operating pressure of 1.5×10^{-2} Pa (1.2×10^{-4} Torr).

Typical anode and keeper voltages were about 21 V and 8.2 V, respectively, relative to cathode potential. Since the plasma potential near the baffle was likely near anode potentials, the baffle was biased 10 V below cathode potential to increase xenon ion energies into the range of those for an NSTAR discharge chamber. This baffle bias also repelled electrons and, therefore, enabled ion current measurements.

Baffle ion currents were 150-162 mA. Baffle volumetric erosion rates were determined by measuring the baffle mass loss after a total accumulated operating time of at least 20 hours, and then dividing by the baffle's material density to convert to a volumetric loss. The varying baffle current was accounted for by dividing this volumetric loss rate by the baffle current.

Initial test results indicate that the volumetric erosion rate of titanium is 17% higher than that of molybdenum at discharge chamber potentials. A post-test analysis of a 30 cm NSTAR ion thruster that was operated for 8200 hours at 2.3 kW only found a slight chamfering of the upstream screen grid apertures from sputter erosion.[3] The chamfering depth, however, never exceeded 11% of the grid thickness. Therefore, given molybdenum's low screen grid erosion at discharge chamber potentials, the 17% higher volumetric erosion rate for titanium is insignificant.

This result is, however, preliminary due to a number of parameters that remain to be examined. For example, although the base pressure was low enough and the baffle current high enough to preclude residual gases in the facility from affecting sputter erosion rates, it is unknown how much material from cathode potential surfaces was sputtered onto the baffle. Furthermore, the energy of incoming xenon ions was not accurately known since no plasma potential measurements were made near the baffle and since the multiply-charge xenon ion content was not measured. These issues should be further investigated.

Material Properties Analyses

A number of material, thermal, and mechanical properties were examined to identify any fabrication, launch environment, and thruster operation issues. The analyses of the following sections do not represent a complete investigation of the aforementioned topics. They are only intended to determine, in general, the suitability of titanium for ion optics.

Material Properties

Material properties for molybdenum and titanium are listed in Table 1. Molybdenum properties are those for the grids on the NSTAR thruster. Titanium properties are those for a commercially-pure titanium grade with high iron and oxygen impurity contents. This grade of titanium was selected for its superior mechanical strength and availability.

There are a number of practical considerations regarding material cost and size availability that were examined. Titanium comes in larger sheet widths than molybdenum (i.e. 61.0 cm for molybdenum versus 91.4 cm for titanium) so that larger diameter optics can be made. Titanium is also 80% cheaper than molybdenum. However, the NSTAR screen grid thickness would have to be increased by about 7% for titanium because this increased size is more readily availability.

Fabrication Issues

The two concerns regarding the fabrication of titanium grids were photo-chemical etching and grid forming characteristics. Titanium is corrosion resistant, a characteristic that makes it difficult to etch. Fortunately, there had been a need by other industries (e.g. medical industry) to develop photo-chemical etching techniques for titanium. As a result, vendors were identified that could photo-chemically etch this material.

Titanium must be ductile enough to be hydrostatically formed. The usual measure of material ductility is elongation, which is listed in Table 1 for both molybdenum and titanium. As the table shows, titanium is 2.5-3x more ductile than molybdenum, so that ductility should not be an issue. However, the high yield strength and low elastic modulus of this grade of titanium results in a greater spring-back following hydrostatic forming. Titanium was calculated to spring-back twice as much as molybdenum, however, spring-back values were within 10% of the final domed height, and, therefore, considered insignificant.

Launch Issues

The two spacecraft launch issues examined were vibration-induced stresses and optics mass. The two vibration-induced stress issues considered were grid plastic deformation and movement. The analysis of vibration-induced stresses and grid movement was complicated by two facts: 1) the shape of the grid will not necessarily be spherical under these stresses; and 2) the grids are perforated. As a result, straightforward calculations were not possible. However, simple comparisons could be made between molybdenum and titanium since the grid geometry would be similar and the g-load would be the same for each material.

Plastic deformation occurs when the vibration-induced stress exceeds the elastic limit stress. Since the elastic limit stress is not typically given in literature, the yield strength at 0.2% offset, listed in Table 1, was used. Grid movement is a function of grid geometry and a grid material's vibration-induced stress, elastic modulus, and Poisson's ratio. Grid vibration-induced stresses are functions of the grid geometry, the g-load

encountered during vibration, and the material density. However, grid geometries and Poisson's ratios are similar, and g-loads are the same for both titanium and molybdenum. Noting that the vibration-induced stresses are directly proportional to the material density, a vibration-induced plastic deformation ratio can be used to compare these materials. This ratio is defined as the vibration-induced stress divided by the yield strength and then normalized for molybdenum:

$$\text{Plastic Deformation Ratio} = \frac{\sigma_{vib}}{\sigma_y} \cdot \frac{\sigma_y^{Mo}}{\sigma_{vib}^{Mo}} = \frac{\rho}{\sigma_y} \cdot \frac{\sigma_y^{Mo}}{\rho^{Mo}} \quad (3)$$

where σ_{vib} and σ_y are vibration-induced stress and the yield stress at 0.2% offset, respectively. A grid movement ratio can be used to compare these materials, where this ratio is defined as the vibration-induced stress divided by the elastic modulus, E, and then normalized for molybdenum:

$$\text{Grid Movement Ratio} = \frac{\sigma_{vib}}{E} \cdot \frac{E^{Mo}}{\sigma_{vib}^{Mo}} = \frac{\rho}{E} \cdot \frac{E^{Mo}}{\rho^{Mo}} . \quad (4)$$

For both ratios, a material is at less risk of plastic deformation and will exhibit less grid movement than molybdenum for ratios less than 1. Using material properties listed in Table 1, titanium was found to have a plastic deformation ratio of 0.60 due to its low density and high yield strength, but a grid movement ratio of 1.4 due to its low elastic modulus. Titanium is, therefore, at less risk of plastic deformation by vibration-induced stresses. However, titanium grids will move more under comparable launch loads. It is unclear whether this increased grid movement for titanium will present a problem.

Since grid geometries for both materials were similar, comparisons of molybdenum and titanium optics masses were made by comparing material densities. Titanium offers a 56% optics mass reduction over molybdenum.

Thruster Operation Issues

Ion thruster optics are operated at high voltages and elevated temperatures. As a result, thermal response, electrostatic pressure, interference with the discharge chamber magnetic circuit, and grid clearing issues were investigated.

MacRae, et al.[9] presented grid temperatures for a 30 cm J-Series ion thruster operating at a 350 W discharge power (which is similar to NSTAR ion thruster operation at full power) with no beam extraction. At equilibrium conditions, temperatures at the centers of the screen and accelerator grids were 353 °C and 292 °C, respectively, with a 61 C° temperature difference. During start-up, this temperature difference was as large as 130 °C. Due to these high temperatures, temperature differences, and the close grid spacing, three thermo-mechanical issues were examined. They include buckling, grid deformation, and plastic deformation.

During thruster operation, the grids will deform due to thermally-induced stresses, which could induce buckling and plastic deformation. The amount of thermally-induced deformation affects thruster operating parameters such as beam divergence, and, therefore, thrust. Grid buckling and plastic deformation can both prevent proper thruster operation and permanently damage the optics. The amount of grid deformation is a function of grid geometry, temperature distribution, and material thermal expansion. Noting that grid geometries are similar for both titanium and molybdenum, titanium grid deformation can be compared to that of molybdenum by comparing their thermal expansion coefficients and assuming similar temperature distributions for both materials. Using values from Table 1, titanium will thermally deform 1.8x more than molybdenum.

Grid buckling can occur if thermal stresses are greater than the critical buckling stress. Grid thermal stresses are functions of the grid geometry, temperature distribution, material elastic modulus, Poisson's ratio and material thermal expansion. The critical buckling stress is a function of grid geometry, Poisson's ratio, and material elasticity modulus. Noting that grid geometries and Poisson's ratios are similar for both titanium and molybdenum and assuming similar temperature distributions for both materials, thermally-induced stresses are directly proportional to:

$$\sigma_{therm} \propto E \cdot \alpha \quad (5)$$

where σ_{therm} is the thermal stress and α is the material linear thermal expansion coefficient. The critical buckling stress is proportional to:

$$\sigma_{cr} \propto E \quad (6)$$

where σ_{cr} is the thermally-induced buckling stress. A buckling parameter can be established:

$$BP = \frac{\sigma_{therm}}{\sigma_{cr}} \quad (7)$$

where buckling occurs only if the buckling parameter, BP, is greater than 1. Titanium can, therefore, be compared to molybdenum by calculating a ratio of the buckling parameters:

$$\text{Buckling Ratio} = \frac{BP}{BP^{Mo}} = \frac{\sigma_{therm}}{\sigma_{cr}} \cdot \frac{\sigma_{cr}^{Mo}}{\sigma_{therm}^{Mo}} = \frac{\alpha}{\alpha^{Mo}} \quad (8)$$

where candidate material has a greater probability of buckling than molybdenum only if the ratio is greater than 1 for a given grid geometry and temperature distribution. Using values from Table 1, this ratio was calculated to be 1.8. Titanium is, therefore, at a greater risk of buckling than molybdenum. This is not surprising since molybdenum has a very small thermal expansion coefficient. Although later sections will show that there were no indications of thermally-

induced buckling up to the NSTAR high power level of 2.3 kW, buckling should be considered at higher power levels where grid temperatures and, therefore, thermally-induced stresses are higher.

Grid plastic deformation occurs when the thermally-induced stress is greater than the elastic limit stress. Since the elastic limit stress is not typically given in literature, the yield strength at 0.2% offset will be used. Thermal stresses are directly proportional to the material elasticity modulus and linear thermal expansion coefficient, as defined above. A thermally-induced plastic deformation parameter can be established:

$$PDP = \frac{\sigma_{therm}}{\sigma_y} \tag{9}$$

where plastic deformation occurs only if the thermally-induced plastic deformation parameter, PDP, is greater than 1. Titanium can, therefore, be compared to molybdenum by calculating a ratio of the of the plastic deformation parameters:

$$\text{Plastic Deformation Ratio} = \frac{PDP}{PDP^{Mo}} = \frac{E \cdot \alpha}{\sigma_y} \cdot \frac{\sigma_y^{Mo}}{E^{Mo} \cdot \alpha^{Mo}} \tag{10}$$

where titanium has a greater risk of plastic deformation than molybdenum if the ratio is greater than 1. Using values from Table 1, this ratio was calculated to be 0.8. Titanium is, therefore, at a lesser risk of thermally-induced plastic deformation than molybdenum due to titanium's high yield strength and low elastic modulus.

To determine if the potential difference between the grids could induce significant grid movement, electrostatic pressure was examined. With a worse-case condition of a 1500 V potential difference and an unusually small 0.254 mm grid spacing, the resulting electrostatic pressure was determined to be 152 Pa (0.022 psi). This was calculated to induce insignificant grid movement, even when material properties were modified to account for grid perforation.[10]

Titanium's magnetic properties were also examined to determine their effect on the discharge chamber magnetic circuit. As shown in Table 1, both titanium and molybdenum are weakly paramagnetic, and, therefore, have no impact on the thruster magnetic circuit.

During long periods of thruster operation, sputter-deposited material, in part from the accelerator grid, will cause electrical shorts between the grids and cause high voltage recycles. It is anticipated that titanium's lower thermal conductivity, higher resistivity, and lower vaporization temperatures would allow larger-sized titanium contaminants to be electrically cleared than those for molybdenum.[11] Furthermore, use of thermally-induced grid displacement techniques to clear grid shorts become more effective with titanium's higher thermal expansion.

Test Setup and Procedures

Titanium Optics

Several titanium grid sets (i.e. matching screen and accelerator grids) were successfully fabricated. A photograph of some titanium grids is shown in Fig. 3. These grid sets were fabricated in two separate lots, with the same screen grid material batch and different accelerator grid material batches used for each lot. The first fabrication lot had a production yield of 40% while the second had a yield 67%. No differences in fabrication lots due to differing accelerator material batches have presently been discerned.

Screen grid aperture diameters were within a 4-11% range of the nominal diameter, which is higher than the 3% range typical of molybdenum screen grids. Accelerator grid aperture diameters were within a 13-24% range of the nominal diameter, which is higher than the 9% range typical of molybdenum accelerator grids. Accelerator apertures were also found to be slightly non-circular under microscopic examination. It is speculated that the large variability of the grid aperture diameters and the non-circular apertures may be the result some aspect of the chemical etching process. It is interesting to note that the most problematic grid (i.e. the accelerator grid) had the smallest apertures etched in the thickest material.

The screen and accelerator grids used for the testing described in this paper had open area fractions that were 6% and 4% larger than the nominal NSTAR designs, respectively. These optics were mounted onto an NSTAR thruster mounting ring assembly, shown in Fig. 3. Although the grid cold gap along the outer perimeter of the active area was set to that of the NSTAR design, the active area mid-radius and center cold gaps were measured to be about 23% larger. This is believed to be the result of higher screen grid yield and tensile strengths, which could have caused the grid to spring-back more than the accelerator grid during hydrostatic forming.

Thruster, Ground Support Equipment, and Operating Procedures

The titanium optics were mounted onto an NSTAR 30 cm engineering model ion thruster which is shown in Fig. 4 and described in detail in ref. 12. This thruster had accumulated about 1000 hours of operation with molybdenum optics.

The thruster was powered by a power console described in ref. 13 that allowed the thruster to be throttled up to 2.3 kW. A high purity gas feed system was used to provide xenon to the discharge cathode,

discharge chamber, and neutralizer through separate mass flow controllers.

Testing was conducted in Vacuum Facility 5 at the NASA Glenn Research Center. The facility is 4.6 m in diameter and 19.2 m in length. Although the facility can be pumped by 19 oil diffusion pumps and a cryogenic pumping system, only 14 oil diffusion pumps were used during these tests. The calculated pumping speed with xenon was approximately 95,000 l/s, with a facility base pressure of 1.7×10^{-4} Pa (1.3×10^{-6} Torr) and background pressures as high as 7.6×10^{-4} Pa (5.7×10^{-6} Torr) at a 2.3 kW thruster input power.

During thruster operation, voltages and currents were measured with digital multimeters. At each beam current, the radial beam current density distribution was measured with a button probe located 1.0 cm downstream from the accelerator grid center. The probe current collecting area was 1.0 cm^2 and was swept on an arc through the grid center with an arc radius of 27.3 cm. The probe was biased negative with respect to beam plasma potential to repel electrons and was grounded through a resistor that acted as a shunt to measure collected currents.

Two tests were conducted. Both tests were designed to measure optics performance. During the first test, the thruster was step-ramped from low to high power at the nominal NSTAR power levels of TH0, TH4, TH8, TH10, TH11, and TH15, which corresponded to nominal thruster input powers, voltages, beam currents, neutralizer currents, and xenon flows listed in Table 2 (a complete listing of NSTAR power levels can be found in ref. 14). At each power level, grid performance parameters such as impingement-limited perveance, electron backstreaming limit, and beam current density distribution, as well as other thruster performance parameters, were measured.

During the second test, the thruster was started from room temperature and immediately brought up to full power (i.e. NSTAR power level TH15). The electron backstreaming limit was then monitored as a function of time. Since the electron backstreaming limit is a strong function of the hot grid gap, this backstreaming limit was used to determine optics thermal behavior.

Results and Discussions

The 30 cm titanium optics on the NSTAR ion thruster operated successfully over the entire NSTAR power range. Thruster behavior was nominal with an average high voltage recycle rate of less than two recycles per hour during steady-state operation.

Impingement-limited perveance and electron backstreaming limit voltages for titanium optics are listed in Table 3 with results from molybdenum optics for comparison. Impingement-limited perveance voltages are also plotted in Fig. 5 as a function of beam current. The impingement-limited perveance voltages were derived from plots of accelerator current as a function of total voltage, shown in Fig. 6, where the slope was -2 mA/100 V. As Table 3 demonstrates, the impingement-limited perveance voltages for titanium optics were greater than those for titanium optics by a factor of 1.11-1.15. The electron backstreaming limit was determined by lowering the magnitude of the accelerator grid voltage until the beam current increased by 1 mA. The magnitude of the electron backstreaming limit voltages for titanium optics were 0.91-0.93x those for molybdenum optics.

These performance differences are likely due to the larger cold gap of the titanium optics at the active area center. The active area center dictates impingement-limited perveance and electron backstreaming limits because both performance parameters are strong functions of the peak beam current density. Beam current densities for the NSTAR thruster are peaked near the active area center, as demonstrated in Fig. 7. The maximum current per aperture is given by the perveance equation:[15]

$$J_b = \frac{\pi \cdot \varepsilon_0}{9} \cdot \sqrt{\frac{2 \cdot q}{m_i}} \cdot V_t^{\frac{3}{2}} \cdot \left(\frac{d_s}{l_e}\right)^2 \qquad (11)$$

where:[16]

$$l_e = \sqrt{\left(l_g + t_s\right)^2 + \left(\frac{d_s}{2}\right)^2}. \qquad (12)$$

Here, J_b is the beamlet current, ε_0 is the permittivity of free space (8.85×10^{-12} $C^2/N\cdot m^2$), q is the charge, m_i is the ion mass, V_t is the total voltage, l_e is the effective acceleration length, d_s is the screen aperture diameter, t_s is the screen grid thickness, and l_g is the hot gap, which will be assumed to be the cold gap. Since beam current density profiles for both molybdenum and titanium are approximately the same, as demonstrated in Fig. 7 at 2.3 kW, the beamlet currents for both grid materials can be equated. It can, therefore, be shown that:

$$\frac{V_t^{Ti}}{V_t^{Mo}} = \left(\frac{l_e^{Ti}}{l_e^{Mo}} \cdot \frac{d_s^{Mo}}{d_s^{Ti}}\right)^{\frac{4}{3}}. \qquad (13)$$

Using nominal NSTAR dimensions for the molybdenum optics and the measured dimensions for the titanium optics, a voltage ratio of 1.11 is calculated, which is similar to those measured in Table 3.

Using a semi-empirical equation derived by Kaufman to solve for the magnitude of the electron backstreaming limit voltage:[17]

$$|V_a| = \frac{0.2 \cdot V_t}{\frac{l_e}{d_a} \cdot \exp\left(\frac{t_a}{d_a}\right)} \qquad (14)$$

where V_a is the accelerator voltage, d_a is the accelerator aperture diameter, and t_a is the accelerator grid thickness. By noting that the accelerator aperture diameters and thicknesses are approximately equal for both materials, it can be shown that:

$$\left|\frac{V_a^{Ti}}{V_a^{Mo}}\right| = \frac{l_e^{Mo}}{l_e^{Ti}}. \quad (15)$$

The above equation yields an accelerator voltage ratio of 0.90, which is similar to the measured values in Table 3. Both this result and that for the impingement-limited perveance indicate that reducing the titanium optics' cold gap at the active area center to the nominal NSTAR gap should eliminate these differences.

Comparisons of accelerator-to-beam current and discharge losses for titanium and molybdenum optics are listed in Table 4. As the table shows, accelerator currents for titanium optics were 1.2x higher than those for molybdenum grids. The higher accelerator currents for the titanium optics were likely caused by an increased direct ion impingement. This increased direct impingement was likely the result of: 1) the titanium optics tested were new while the molybdenum optics used for comparison had been operated for some time and were "burned-in"; and 2) poor optics alignment. Regarding the former cause, new optics tend to have higher-than-normal impingement currents. After accumulating some operating time, accelerator grid apertures become sputter-eroded, and the impingement current tends to decrease rapidly. This is demonstrated in ref. 3 and 18, where NSTAR thruster accelerator currents decreased by as much as 50% within the first 1500 hours of life testing, after which they remained nearly constant. Unfortunately, no impingement current data for new molybdenum optics at similar background pressures and operating conditions were available for comparison.

Table 4 also shows that discharge losses for titanium grids were 0.9x those for molybdenum. This improvement was likely due to the slightly larger titanium screen grid open area fraction.

Radial distributions of beam current density with titanium optics were very similar to those with molybdenum optics at all power levels. This is demonstrated in Fig. 7, which compares radial beam current density distributions for both titanium and molybdenum optics at 2.3 kW (i.e. a beam current of 1.76 A). Table 3 also shows that the peak beam current densities for both titanium and molybdenum optics were very similar. No radial beam current density distribution gave any indication of thermally-induced buckling.

Fig. 8 shows the electron backstreaming limit voltage difference (i.e. the temporal value minus the final equilibrium value) as a function of time for both titanium and molybdenum optics, where the thruster was set to 2.3 kW immediately following ignition from room temperature. The electron backstreaming limit voltage is a function of grid gap, therefore, the time required for this limit voltage to stabilize approximates the time required for the electrodes to achieve thermal equilibrium. The data in Fig. 8 for both molybdenum and titanium optics show that the screen grid heats up much faster than the accelerator grid, probably because the screen grid has a considerably smaller thermal mass and is enclosed within the thruster. As a result, the screen grid dome height initially increases more than that of the accelerator grid, thereby reducing the hot gap, especially at the grid center. Further heating increases the accelerator grid height until the hot gap stabilizes and thermal equilibrium is achieved. Fig. 8 shows that the titanium optics achieved thermal equilibrium about 10 minutes faster than molybdenum optics.

Future work should include reducing the grid gap at the active area center and repeating the aforementioned tests. Since titanium's higher thermally-induced grid deformation can affect beam divergence and thrust, far-field beam current densities and thrust should be measured. To address grid movement from vibration-induced stresses, titanium optics should be vibration-tested. Fabrication issues such as the slightly non-circular accelerator grid apertures should also be investigated. Finally, titanium optics should be wear-tested on a 30 cm ion thruster to demonstrate improved total impulse capability.

Conclusions

A development effort was initiated to identify a material with a lower accelerator grid volumetric sputter erosion rate than molybdenum, but that could utilize the present NSTAR thruster grid design and fabrication techniques to keep development costs low, and perform as well as molybdenum optics. After having compared the sputter erosion rates of several atomic materials to that of molybdenum at typical accelerator voltages, titanium was found to offer a 45% reduction in volumetric erosion rates and could be made with the existing grid fabrication process.

To ensure that screen grid sputter erosion rates would not limit thruster total impulse capability, erosion rate measurements were made on titanium and molybdenum samples in a simple xenon discharge. Preliminary results showed only a slightly higher volumetric erosion rate for titanium, so that screen grid erosion is insignificant.

A number of material, thermal, and mechanical properties were also examined to identify any fabrication, launch environment, and thruster operation issues. Titanium was found to come in larger sheet widths than molybdenum so that larger diameter optics

can be made, and was also found to be cheaper than molybdenum. Although the present NSTAR screen grid thickness had to be increased by 7% because this size was more readily available, titanium's lower density allowed for a 56% reduction in optics mass. Although titanium was at less risk for plastic deformation than molybdenum under launch and thermally-induced stresses during thruster operation, grid movement would be greater under launch loads. The risk of thermally-induced grid buckling during thruster operation would be increased, however, testing demonstrated that this was not a problem. Grid movement under electrostatic pressure and interference with the discharge chamber magnetic circuit were also found to be insignificant, while grid short clearing was improved for titanium.

Several titanium grid sets were successfully fabricated. Both screen and accelerator grids exhibited a larger variability in aperture diameters than with molybdenum and accelerator grid apertures were slightly non-circular.

The titanium optics were mounted onto an NSTAR 30 cm engineering model ion thruster and tested to determine optics performance. The titanium optics operated successfully over the entire NSTAR power range of 0.5 to 2.3 kW. Impingement-limited perveance voltages and the magnitude of the electron backstreaming limit voltages for molybdenum optics were greater than and less than those for titanium optics, respectively. Both differences could be explained by a larger cold gap for the titanium optics. Such differences could be eliminated by reducing the titanium optics' cold gap at the active area center to the nominal NSTAR gap.

Although accelerator currents for titanium optics were higher than those for molybdenum grids, this increase was likely the result of poor optics alignment and the fact that the molybdenum optics used for comparison were "burned-in" and not new. Discharge losses for titanium grids were lower than those for molybdenum, likely due to the slightly larger titanium screen grid open area fraction. Radial distributions of beam current density with titanium optics were very similar to those with molybdenum optics at all power levels.

Electron backstreaming limit was measured as a function of elapsed time from ignition. Since the electron backstreaming limit is a strong function of the hot grid gap, the time required for this limit voltage to stabilize approximated the time required for the grids to achieve thermal equilibrium. Titanium optics achieved thermal equilibrium about 10 minutes faster than molybdenum optics.

References

[1] Rawlin, V.K., et al. "An Ion Propulsion System for NASA's Deep Space Missions," AIAA Paper 99-4612, September 1999.

[2] Polk, J.E., et al., "Validation of the NSTAR Ion Propulsion System on Deep Space One Mission: Overview and Initial Results," AIAA Paper 99-2274, June 1999.

[3] Polk, J.E., et al., "An Overview of the Results from an 8200 Hour Wear Test of the NSTAR Ion Thruster," AIAA Paper 99-2446, June 1999.

[4] Rawlin, V.K., "Erosion Characteristics of Two-Grid Ion Accelerating Systems," IEPC Paper 93-175, September 1993.

[5] Rawlin, V.K., Banks, B.A., and Byers, D.C., "Design, Fabrication, and Operation of Dished Accelerator Grids on a 30-cm Ion Thruster," AIAA Paper 72-486, April 1972.

[6] Rosenberg, D. and Wehner, G.K., "Sputtering Yields for Low Energy He^+-, Kr^+-, and Xe^+-Ion Bombardment," Journal of Applied Physics, vol. 33, no. 5, pp. 1842-1845, May 1962.

[7] Blandino, J.J., et al., "Evaluation of Diamond Grids for Ion Thruster Optics: Low Energy Sputter Yield Measurements," AIAA Paper 96-3203, July 1996.

[8] Poeschel, R.L. et al., "High-Power and 2.5 kW Advanced-Technology Ion Thruster," NASA Contractor Report 135163, Hughes Research Laboratories, February 1977.

[9] MacRae, G.S., Zavesky, R.J., and Gooder, S.T., "Structural and Thermal Response of 30 cm Diameter Ion Thruster Optics," AIAA Paper 89-2719, Jul. 1989.

[10] Horvay, G., "The Plane-Stress Problem of perforated Plates," Journal of Applied Mechanics, vol. 19, pp. 355-360, September 1952.

[11] Goodfellow, K.D., Ganapathi, G.B., and Stocky, J.F., "An Experimental and Theoretical Analysis of the Grid Clearing Capability of the NSTAR Ion Propulsion System," AIAA Paper 99-2859, June 1999.

[12] Sovey, J.S., et al., "Development of an Ion Thruster and Power Processor for New Millennium's Deep Space 1," AIAA Paper 97-2778, December 1997.

[13] Pinero, L.R., Patterson, M.J., and Satterwhite, V.E., "Power Console Development for NASA's Electric Propulsion Outreach Program," IEPC Paper 93-250, September 1993.

[14] Rawlin, V.K., et al., "NSTAR Flight Thruster Qualification Testing," AIAA Paper 98-3936, July 1998.

[15] Rawlin, V.K., "Characterization of Ion Accelerating Systems on NASA LeRC's Ion Thrusters," AIAA Paper 92-3827, July 1992.

[16] Patterson, M.J., "Low-Isp Derated Ion Thruster Operation," AIAA Paper 92-3203, July 1992.

[17] Kaufman, H.R., "Technology of Electron Bombardment Ion Thrusters," Advances in Electronics and Electron Physics, vol. 36, Academic Press, Inc., New York, 1974, pp. 265-373.
[18] Anderson, J.R., et al., "Results of an On-going Long Duration Ground Test of the DS1 Flight Spare Ion Engine," AIAA Paper 99-2857, June 1999.
[19] Weast, R.C., ed., CRC Handbook of Chemistry and Physics, 62nd edition, CRC Press, Inc., 1981.
[20] Anon., "Molybdenum Metal," CSM Industries Internal Report, 1960.
[21] Boyer, R., Welsch, G., and Collings, E.W., ed., Materials Property Handbook: Titanium Alloys, ASM International, 1994, pp. 165-260.

Table 1. Material properties for molybdenum and titanium.

Material Property	Molybdenum[a]	Titanium[b]
Atomic Mass, amu	95.94	47.90
Density, gm/cm^3	10.22	4.51
Thermal Properties		
Melting Point, °C	2610	1650-1670
Thermal Conductivity, W/m·K	145 (0 °C)	17.4 (20 °C)
	136 (200 °C)	16.9 (205 °C)
	128 (400 °C)	17.3 (425 °C)
Thermal Expansion, µm/m·K	5.1	9.2
	(20-540 °C)	(0-540 °C)
Total Hemispherical Emittance	0.08 (200 °C)	0.30 (200 °C)
	0.09 (400 °C)	0.30 (400 °C)
	0.11 (600 °C)	0.31 (600 °C)
Electrical Properties		
Resistivity (µΩ·cm)	5.2 (0 °C)	42.0 (20 °C)
	11 (200 °C)	82 (200 °C)
	15 (400 °C)	114 (400 °C)
Magnetic Properties		
Magnetic Susceptibility at 20 °C, mks	120×10^{-6}	180×10^{-6}
Mechanical Properties		
Elastic Modulus, GPa (10^6 psi)	324 (47)	104 (15.1)
Tensile Strength,[c] MPa (ksi)	795 (115)	552 (80.0)
Yield Strength @ 0.2% Offset,[c] MPa (ksi)	655 (95)	483 (70.0)
Elongation (%)	5-6	15
Poisson's Ratio (25 °C)	0.32	0.34-0.40

[a]Molybdenum material properties are for the stress-relieved condition; data from ref. 19 and 20.
[b]Titanium and niobium properties are for the annealed condition; data from ref. 19 and 21.
[c]Ultimate tensile and yield strength properties are minimum required values.

Table 2. Nominal thruster operating parameters.

NSTAR Power Level	Input Power,[a] kW	Beam Current, A	Beam Voltage,[b] V	Accelerator Voltage,[c] V	Neutralizer Keeper Current, A	Main Flow, sccm	Discharge Cathode Flow, sccm	Neutralizer Flow, sccm
TH0	0.5	0.51	650	-150	2.0	5.98	2.47	2.40
TH4	1.0	0.71	1100	-150	2.0	8.30	2.47	2.40
TH8	1.4	1.10	1100	-180	1.5	14.4	2.47	2.40
TH10	1.7	1.30	1100	-180	1.5	17.2	2.56	2.49
TH11	1.8	1.40	1100	-180	1.5	18.5	2.72	2.65
TH15	2.3	1.76	1100	-180	1.5	23.4	3.70	3.60

[a]Nominal values.
[b]Power supply voltage.
[c]When starting the thruster from a cold condition, accelerator voltage is initially set to -250 V for 2 hours to prevent electron backstreaming from transient heating of the optics.

Table 3. Titanium and molybdenum optics performance.

NSTAR Power Level	Beam Current, A	Peak Beam Current Density, mA/cm^2		Impingement-Limited Total Voltage, V			Electron Backstreaming Limit, V		
		Ti	Mo[a]	Ti	Mo[b]	Vt^{Ti}/Vt^{Mo}	Ti	Mo[b]	Va^{Ti}/Va^{Mo}
TH0	0.50	2.9	3.2	750	660	1.14	-60	-66	0.91
TH4	0.71	4.0	4.1	840	740	1.14	-111	-121	0.92
TH8	1.10	5.4	5.6	990	860	1.15	-125	-134	0.93
TH10	1.30	5.9	6.2	1035	920	1.13	-128	-140	0.91
TH11	1.40	6.2	-	1070	-	-	-133	-	-
TH15	1.76	6.8	7.0	1170	1050	1.11	-143	-154	0.93

[a] Data from same engineering model thruster with NSTAR molybdenum grids operated in Vacuum Facility 5.
[b] Data from ref. 14, Flight Thruster 1, first functional test at GRC.

Table 4. Ion thruster test results with titanium and molybdenum optics at similar background pressures.

NSTAR Power Level	Beam Current, A	Accelerator Current, mA	Accelerator-to-Beam Current, %			Discharge Losses,[a] W/A		
			Ti	Mo[b]	Ti/Mo	Ti	Mo[c]	Ti/Mo
TH0	0.50	2.2	0.44	-	-	241	268	0.90
TH4	0.71	3.0	0.42	0.34	1.24	222	252	0.88
TH8	1.10	5.7	0.52	0.43	1.21	198	218	0.91
TH10	1.30	7.0	0.54	0.46	1.17	189	-	-
TH11	1.40	8.4	0.60	-	-	189	-	-
TH15	1.76	11.3	0.64	0.52	1.23	188	207	0.91

[a] Assume only singly-charged ions.
[b] Data from same engineering model thruster with NSTAR molybdenum grids operated in Vacuum Facility 5 at similar background pressures.
[c] Data from same engineering model thruster with new NSTAR molybdenum grids operated in Vacuum Facility 5.

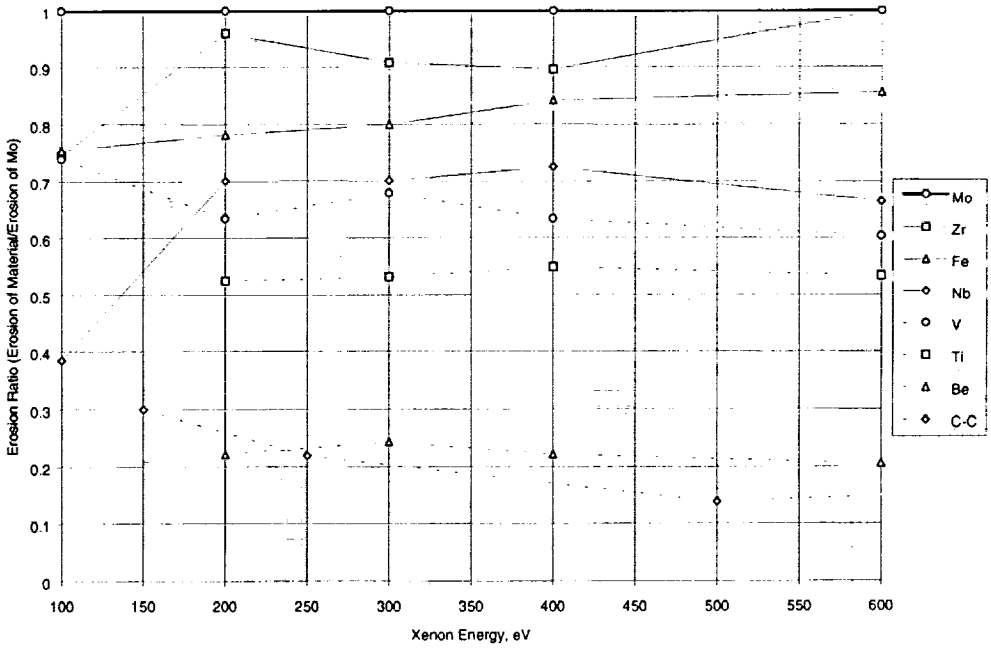

Fig. 1. Erosion ratios of various materials as a function of xenon ion energy. Data from ref. 6 and 7.

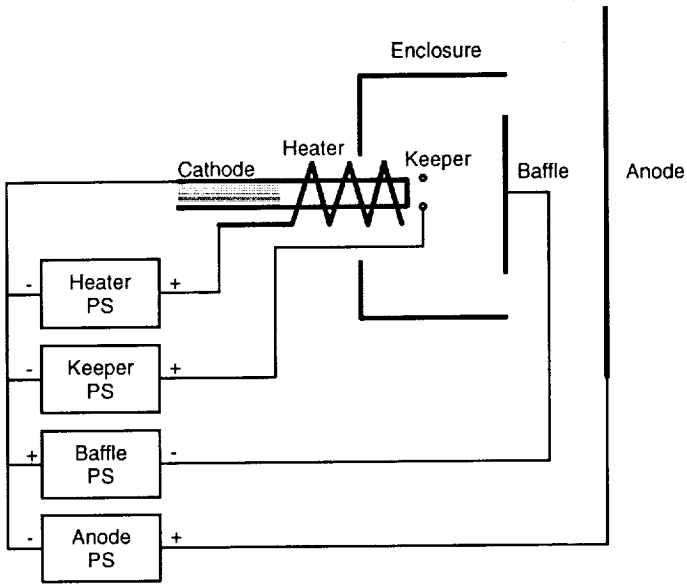

Fig. 2. Experimental setup for measurements of low energy sputter erosion rates.

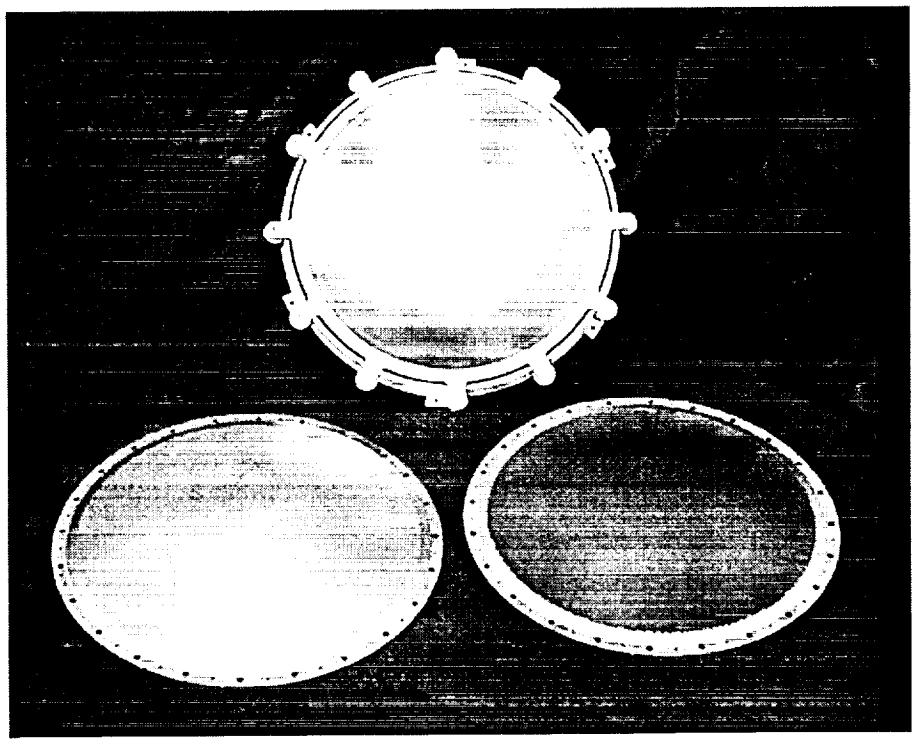

Fig. 3. Photograph of titanium grids with and without the thruster mounting ring.

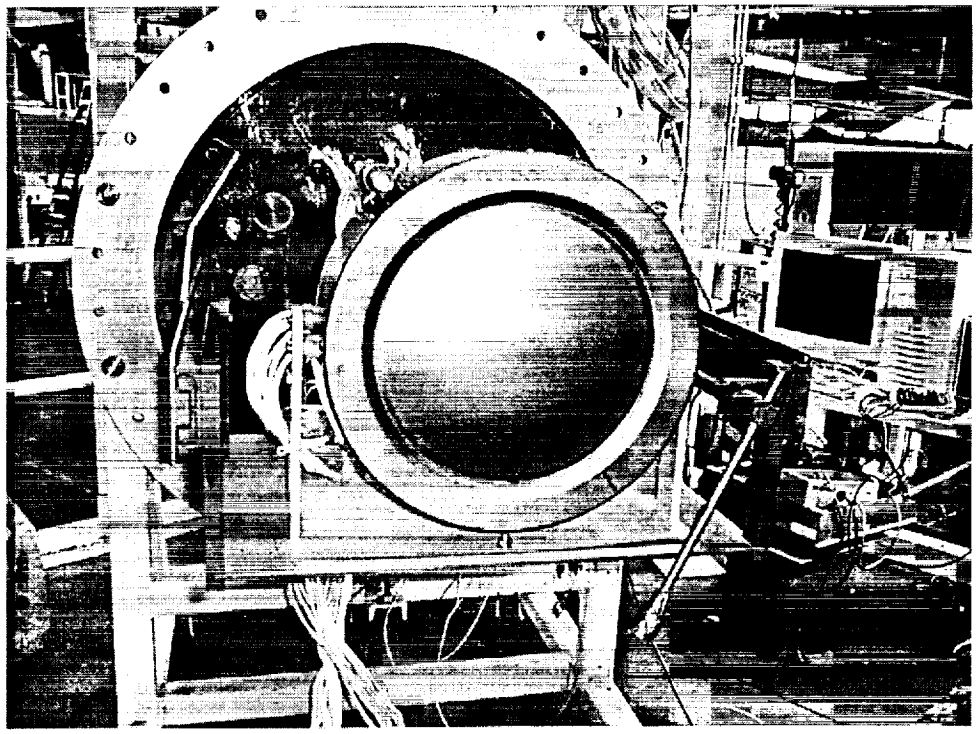

Fig. 4. Titanium optics installed onto an NSTAR engineering model ion thruster.

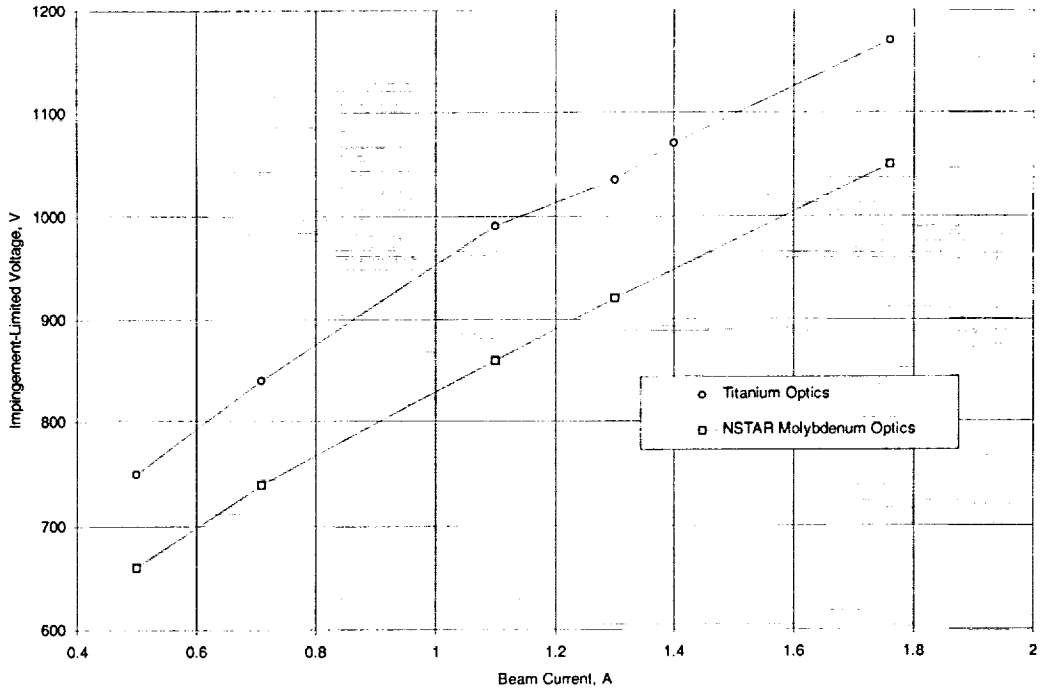

Fig. 5. Impingement-limited perveance voltage (i.e. total voltage) as a function of beam current. Molybdenum optics test results are from NSTAR optics operated on the same engineering model thruster.

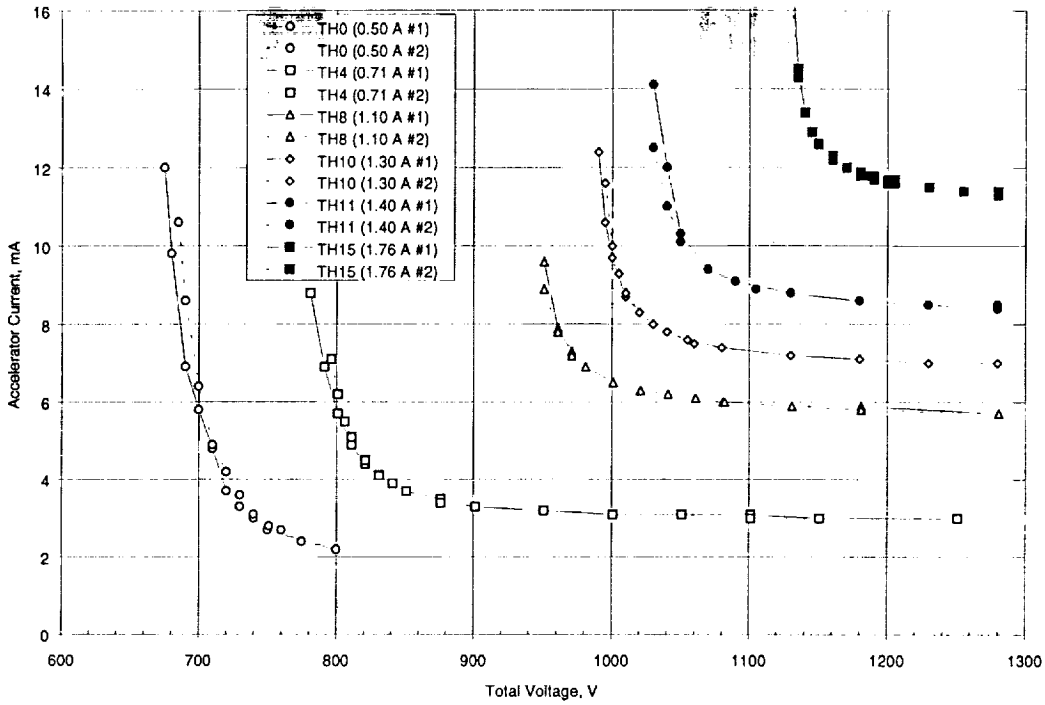

Fig. 6. Accelerator current as a function of total voltage.

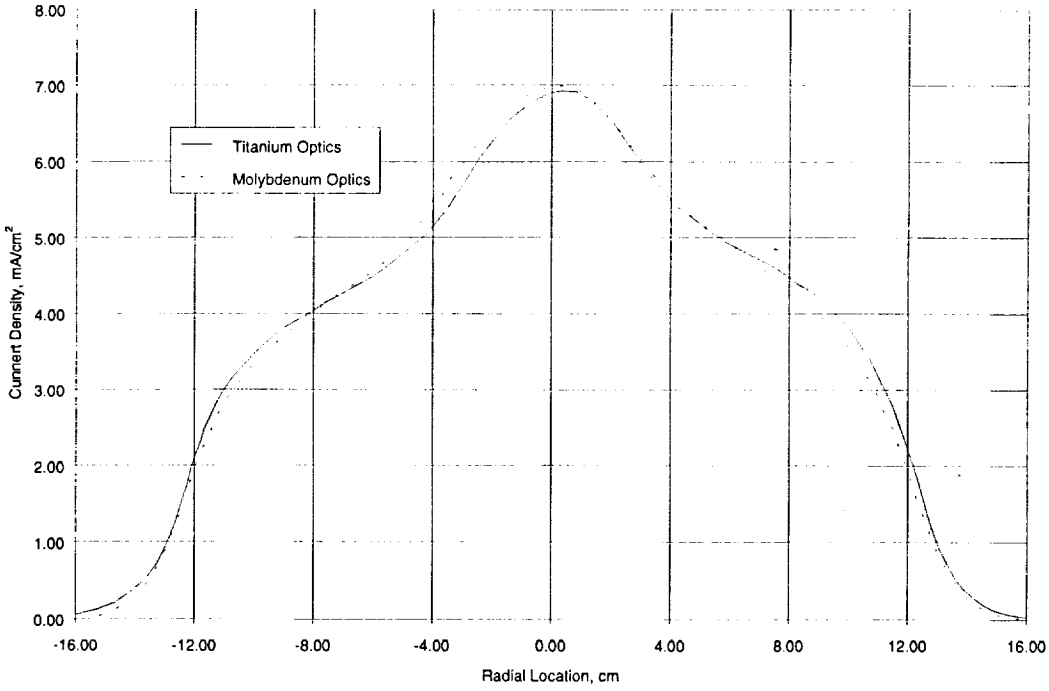

Fig. 7. Beam current density profiles for both titanium and molybdenum optics at a 1.76 A beam current and a 2.3 kW nominal input power. Molybdenum optics test results are from NSTAR optics operated on the same engineering model thruster.

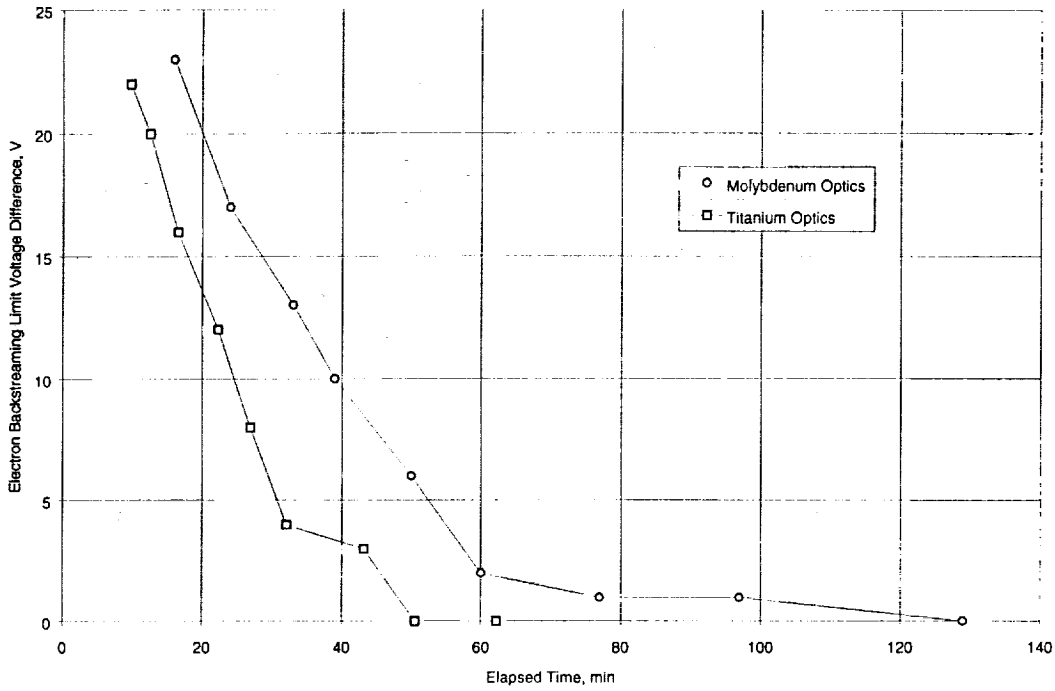

Fig. 8. Electron backstreaming voltage limit difference (i.e. temporal value – final equilibrium value) as a function of elapsed time for titanium and molybdenum optics at a 2.3 kW nominal input power. Molybdenum optics test results are from Flight Thruster 1 optics of ref. 14.

REPORT DOCUMENTATION PAGE

Form Approved
OMB No. 0704-0188

1. AGENCY USE ONLY (*Leave blank*)	2. REPORT DATE	3. REPORT TYPE AND DATES COVERED
	December 1999	Technical Memorandum

4. TITLE AND SUBTITLE

Titanium Optics for Ion Thrusters

5. FUNDING NUMBERS

WU–632–1B–1B–00

6. AUTHOR(S)

George C. Soulas, Thomas W. Haag, Michael J. Patterson, and Vincent K. Rawlin

7. PERFORMING ORGANIZATION NAME(S) AND ADDRESS(ES)

National Aeronautics and Space Administration
John H. Glenn Research Center at Lewis Field
Cleveland, Ohio 44135–3191

8. PERFORMING ORGANIZATION REPORT NUMBER

E–12004

9. SPONSORING/MONITORING AGENCY NAME(S) AND ADDRESS(ES)

National Aeronautics and Space Administration
Washington, DC 20546–0001

10. SPONSORING/MONITORING AGENCY REPORT NUMBER

NASA TM—1999-209650
IEPC 99–149

11. SUPPLEMENTARY NOTES

Prepared for the 26th International Electric Propulsion Conference sponsored by the American Instittue of Aeronautics and Astronauites, Kitakyushu, Japan, October 17–21, 1999. George C. Soulas, Dynacs Engineering Company, Inc., 2001 Aerospace Parkway, Brook Park, Ohio 44142; Thomas W. Haag, Michael J. Patterson, and Vincent K. Rawlin, NASA Glenn Research Center. Responsible person, Thomas W. Haag, organization code 5430, (216) 977–7423.

12a. DISTRIBUTION/AVAILABILITY STATEMENT

Unclassified - Unlimited
Subject Category: 20 Distribution: Nonstandard

This publication is available from the NASA Center for AeroSpace Information, (301) 621–0390.

12b. DISTRIBUTION CODE

13. ABSTRACT ***(Maximum 200 words)***

Ion thruster total impulse capability is limited, in part, by accelerator grid sputter erosion. A development effort was initiated to identify a material with a lower accelerator grid volumetric sputter erosion rate than molybdenum, but that could utilize the present NSTAR thruster grid design and fabrication techniques to keep development costs low, and perform as well as molybdenum optics. After comparing the sputter erosion rates of several atomic materials to that of molybdenum at accelerator voltages, titanium was found to offer a 45% reduction in volumetric erosion rates. To ensure that screen grid sputter erosion rates are not higher at discharge chamber potentials, titanium and molybdenum sputter erosion rates were measured at these potentials. Preliminary results showed only a slightly higher volumetric erosion rate for titanium, so that screen grid erosion is insignificant. A number of material, thermal, and mechanical properties were also examined to identify any fabrication, launch environment, and thruster operation issues. Several titanium grid sets were successfully fabricated. A titanium grid set was mounted onto an NSTAR 30 cm engineering model ion thruster and tested to determine optics performance. The titanium optics operated successfully over the entire NSTAR power range of 0.5 to 2.3 kW. Differences in impingement-limited perveances and electron backstreaming limits were found to be due to a larger cold gap for the titanium optics. Discharge losses for titanium grids were lower than those for molybdenum, likely due to a slightly larger titanium screen grid open area fraction. Radial distributions of beam current density with titanium optics were very similar to those with molybdenum optics at all power levels. Temporal electron backstreaming limit measurements showed that titanium optics achieved thermal equilibrium faster than molybdenum optics.

14. SUBJECT TERMS	15. NUMBER OF PAGES
Ion thruster; Ion optics; Grids	20
	16. PRICE CODE: A03

17. SECURITY CLASSIFICATION OF REPORT	18. SECURITY CLASSIFICATION OF THIS PAGE	19. SECURITY CLASSIFICATION OF ABSTRACT	20. LIMITATION OF ABSTRACT
Unclassified	Unclassified	Unclassified	